Particle Accelerators, Vol. 60, pp. 103–120
Reprints available directly from the publisher
Photocopying permitted by license only

XPS CHARACTERIZATION OF NIOBIUM FOR RF CAVITIES

A. DACCÀ[a,*], G. GEMME[a], L. MATTERA[b] and R. PARODI[a]

[a]*INFN – Sezione di Genova, Via Dodecaneso 33, I-16146 Genova, Italy;*
[b]*Unità INFM – Dipartimento di Fisica, Università degli Studi di Genova, Via Dodecaneso 33, I-16146 Genova, Italy*

(Received in final form 15 January 1998)

Niobium utilization for the realization of RF devices is nowadays very common; nevertheless there are still many problems concerning the achievement of the critical magnetic field and the reduction of the surface resistance, produced principally by surface contamination. A first solution of these problems is constituted by a series of surface treatments, among which there are the thermal treatments. The consequences of thermal treatments (in the range 30–1000°C) on niobium surface exposed to different preparations have been analysed by XPS and ARXPS. During the heating phase an irreversible transition has been observed near $T = 200$–300°C; it is characterized by a progressive reduction of niobium oxides from Nb_2O_5 to NbO_2 and finally to NbO. The oxygen signal disappears near $T = 1000$°C and it reappears below 900°C, during the cooling phase. This can be interpreted as due to oxygen migration in the niobium matrix, raising T, and to oxygen diffusion towards the surface as the temperature decreases.

Work function measurements have been performed and the Φ values have been correlated with the chemical surface composition.

All these processes are of primary importance in understanding the correlation between the chemical composition of the surface and the secondary electron emission occurring inside superconducting cavities.

Keywords: Superconductivity; Radiofrequency; Cavities; XPS

1. INTRODUCTION

Niobium is, at the present, the most widely used material in the realization of superconducting radiofrequency (RF) cavities, even if the

* Corresponding author. Tel.: +39-10-3536346. Fax: +39-10-313378.
E-mail: DACCA@GE.INFN.IT.

problems related to the achievement of the critical magnetic field B_c[1–3] and the residual resistance R_{res}[1–3] are still unsolved.

It is well recognized that the residual resistance, whose value is temperature independent and that strongly affects the quality factor Q, is produced by structural imperfections and surface impurities, like oxygen and carbon, so that a series of surface treatments, both chemical and thermal, have been developed to reduce surface contamination.[4]

As far as thermal treatment concerns, an exhaustive and systematic study on niobium is still necessary to understand the major mechanisms operating on the surface during a thermal cycle. A group of authors[5,6] found that temperatures near 1800°C are necessary to eliminate contamination produced by oxygen, since the evaporation of niobium oxides from the surface begins only above 1600°C, while below these temperatures oxygen atoms tend to migrate into the niobium matrix. This is one of the reasons for which a thermal treatment at 1400–1600°C is performed on niobium cavities.

The aim of the present work is to investigate the consequences of thermal treatments in the range 30–1000°C on the surface chemical composition of niobium by means of X-ray Photoelectron Spectroscopy (XPS) and Angle Resolved X-ray Photoelectron Spectroscopy (ARXPS).

We also performed work function measurements during ion sputtering profiles, in order to correlate the value of the work function with the different compounds present on the surface. These results give insights on the relation between the electron emission process and the chemical composition of the first atomic layers.

2. EXPERIMENTAL

A. Spectrometer

Measurements on niobium samples are performed in a PHI ESCA 5600ci MultiTechnique electron spectrometer. A base pressure of 2×10^{-10} Torr is obtained, in the analysis chamber, by a combination of turbomolecular, ion and titanium sublimation pumps; the residual gas in the analysis chamber is composed of H_2 and H_2O and, to a lower extent, of CO, Ar and CO_2.

The spectrometer is provided with a standard MgKα source ($h\nu = 1253.6$ eV) and a monochromatized AlKα source ($h\nu = 1486.6$ eV), an SCA (Spherical Capacitor Analyzer) electron energy analyzer, with an energy resolution of 0.5 eV, an ion gun, that produces a beam of Ar ions in the energy range between 2 and 5 KeV, a residual gas analyzer and a fast entry lock for the introduction of the specimen.

The sample holder system is equipped with a heater (a tantalum filament wrapped on a ceramic mount) that allows to reach 1000°C and a copper bar in thermal contact with a liquid nitrogen dewar for cooling the sample. The heating and cooling rates are different according to the different ranges of temperature at which the filament operates. In the heating phase, under 800°C, the heating rate is of the order of ≈ 0.5°C/s, while above 800°C it decreases to ≈ 0.2°C/s; in the cooling phase the rate is of the order of ≈ 0.7°C/s for $T > 300$–400°C, and it decreases to ≈ 0.08°C/s under 300°C.

The electron energy analyzer operates in the constant energy mode at a pass energy of 2.95 eV for ARXPS measurements and of 11.75 eV for XPS measurements. The binding energy values are measured with an accuracy of ± 0.1 eV.

All spectra are recorded by sampling an area of 400 μm/diameter; the acceptance angle is of $\pm 7°$ for XPS measurements and of $\pm 2°$ for ARXPS measurements.

In XPS measurements electrons emitted at a take-off angle of 45° are analyzed.

To evaluate the thickness of the compounds present on the surface we have performed an angle-resolved analysis at every fixed temperature.

Work function values Φ are obtained by measuring the total width of the photoelectron spectrum.

Depth profile analysis is performed by alternating XPS spectra and Φ measurements with ion sputtering (Ar^+ at 2 keV).

B. Sample Preparation

XPS measurements are performed on niobium samples obtained from the same plate we use to make RF cavities.[7] This is polycrystalline niobium (linear grain size ≈ 2–4 mm) of 99.95% purity

TABLE I Different treatments applied to niobium to obtain four samples for XPS analysis

Sample	*Treatments*	*Parameters*
1	Air exposure	$t = 20$ min
2	Chemical polishing	$HNO_3 : HF : H_3PO_4 = 1 : 1 : 1$ 18°C T_{ROOM}
3	5 V anodization	$NH_4OH : H_2 = 7 : 100$ 5 V T_{ROOM}
4	20 V anodization	$NH_4OH : H_2 = 7 : 100$ 20 V T_{ROOM}

with 300 ppm of tantalum and with a RRR (residual resistivity ratio) ≈ 200.

In order to eliminate any possible contribution coming from chemical composition or geometry, we have employed the same specimen (a disk of 20 mm diameter and 5 mm height) to prepare all samples which will be discussed in the present work. All samples were chemically polished first in a 1 : 1 : 1 solution of HNO_3, HF and H_3PO_4. This treatment at $T = 18$°C for $t = 2.5$ min removes 20 μm of material[8] allowing to eliminate from the surface any trace of mechanical machining (or of any previous treatment). After this "basic" treatment, different samples were prepared following procedures commonly employed in the preparation of RF cavities; these samples are listed in Table I.

In particular we describe in detail the results obtained on the sample anodized at 5 V; the anodization results in the growth, on the niobium surface, of a Nb_2O_5 layer whose thickness depends on the voltage applied to the cell ($\cong 0.8$–1 nm/V).[9] An overview of the characteristics observed for other preparations of the sample will be given in Sections 4–5.

C. XPS and ARXPS analyses

The first XPS analysis performed on all samples is the acquisition of a complete XPS spectrum (a "survey" spectrum) in order to identify the chemical species present on the surface. The next step is the deconvolution of the peak shape for the identification of the different chemical states which produce that XPS signal.

In the case of a conducting material the line shape is obtained by the convolution of the Doniach and Sunjic curve,[10] representing the intrinsic shape of the line, with a Gaussian curve, which takes into

account instrumental effects. The deconvolution of the measured lines is then performed by using asymmetric Gaussian–Lorentzian functions.[11]

To determine the atomic concentration X of the different compounds, we have to consider the expression of the intensity I of an XPS line j at kinetic energy E produced by an element A in an homogeneous sample Z:[12]

$$I_A(j,Z) = T(E) \times D(E) \times \Sigma \times I_0(h\nu) \times \Delta\Omega \times N_Z \times \lambda_Z(E) \times \cos\varphi \times \frac{d\sigma(j,A)}{d\Omega} \times X_A(Z), \quad (1)$$

where $T(E)$ is the transmission function and $D(E)$ is the detection efficiency of the analyzer; $D(E)$ is a constant for electron energy analyzer that operates at constant pass energy. In Eq. (1), Σ is the area analyzed, $I_0(h\nu)$ is the X-ray flux at energy $h\nu$, $\Delta\Omega$ is the solid angle of acceptance of the analyzer, N_Z is the atomic density of the sample, $\lambda_Z(E)$ is the attenuation length for a photoelectron of energy E in the material Z, $X_A(Z)$ is the atomic concentration of element A in the compound Z, φ is the electron take-off angle relative to the normal to the sample and $d\sigma(j,A)/d\Omega$ is the differential photoelectron cross-section relative to the line j of element A.

The intensity of each XPS line is calculated as the area under the peak after a proper background subtraction with the method of Shirley.[13]

If we consider the intensity ratio of two elements A and B, all terms that are constant for a particular geometry (Σ, $I_0(h\nu)$, $\Delta\Omega$, $\cos\varphi$) cancel out:

$$\frac{I_A}{I_B} = \frac{S_A X_A}{S_B X_B}. \quad (2)$$

In Eq. (2), S_i is the sensitivity factor for the ith element and it is given by:

$$S_i = N_i \times \lambda_i(E_i) \frac{d\sigma(j,i)}{d\Omega} \times \frac{1}{E_i}, \quad (3)$$

where the $1/E$ dependence of S_i is produced by the energy dependence of the transmission function of the analyzer. In this work we use the

sensitivity factors of the *Handbook of Photoelectron Spectroscopy*[14] that are all normalized to the 1s line of fluorine.

Therefore the expression for the calculation of the atomic concentration of an element A is:

$$X_A = \frac{I_A/S_A}{\sum_{i=1}^{N} I_i/S_i}, \tag{4}$$

where N is the number of elements detected on the surface.

Taking advantage of the dependence of the photoelectrons escape depths with take-off angle (Figure 1), it is possible to determine the in-depth composition by means of an angle-resolved XPS analysis.

This kind of measurement allows to evaluate film thickness. In the case of an overlayer A on a substrate B, the thickness d_A of the overlayer is given by[15]

$$d_A = \lambda_A \sin\theta \times \ln\left(\frac{X_A(\theta)}{X_B(\theta)} + 1\right), \tag{5}$$

where $X_A(\theta)$ and $X_B(\theta)$ are the concentrations of species A and B measured at the angle of emission θ relative to the surface of the sample. Obviously, Eq. (5) can be applied only if $d_A < 3\lambda_{A,B}$ where $\lambda_{A,B}$ are the escape depths of electrons generated from the lines used to detect species A and B, respectively. Considering the energy of the incoming photons and the XPS lines to which we are interested

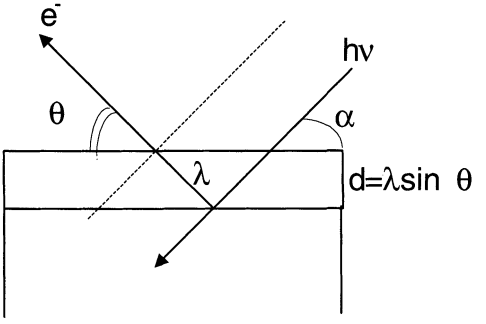

FIGURE 1 Dependence of the photoelectron escape-depth d on the take-off angle θ; λ is the elastic mean free path and α is the angle of incidence of X-ray with respect to the surface plane.

TABLE II Values of the attenuation length λ calculated with Eqs. (6)–(8); in the first column in parentheses there is the XPS line considered for the evaluation of λ. In the second column there is the dimension of the atom or of the compound, in the third the kinetic energy corresponding to the XPS line considered and in the last column the values of λ

Compound	a (nm)	E (eV)	λ (nm)
Nb (Nb3d)	0.32	1281	2.5
NbO (Nb3d)	0.33	1270	3.7
NbO_2 (Nb3d)	0.33	1277.2	3.7
Nb_2O_5 (Nb3d)	0.45	1275.7	5.8
NbC (C1s)	0.33	1201.2	4.7
Graphite (C1s)	0.35	1199.2	2.9

(Nb3d, O1s and C1s), the escape depths are of the order of $3\lambda \leq$ 60–80 Å, where the equal sign holds at normal emission.

The values of the attenuation length have been calculated by using the expressions of Seah and Dench:[16]

for elements

$$\lambda = \frac{538}{E^2} + 0.41\sqrt{aE} \quad \text{(nm)}; \tag{6}$$

for oxides

$$\lambda = \frac{2170}{E^2} + 0.55\sqrt{aE} \quad \text{(nm)}; \tag{7}$$

for inorganic compounds

$$\lambda = \frac{2170}{E^2} + 0.72\sqrt{aE} \quad \text{(nm)}; \tag{8}$$

where E, in eV, is the kinetic energy relative to XPS line of the element considered and a, in nm, is the dimension of the atom or compound. The values of λ used in this work are reported in Table II.

3. RESULTS

A. Heating Phase

Results about XPS measurements during the heating phase are summarized in Figures 2–4.

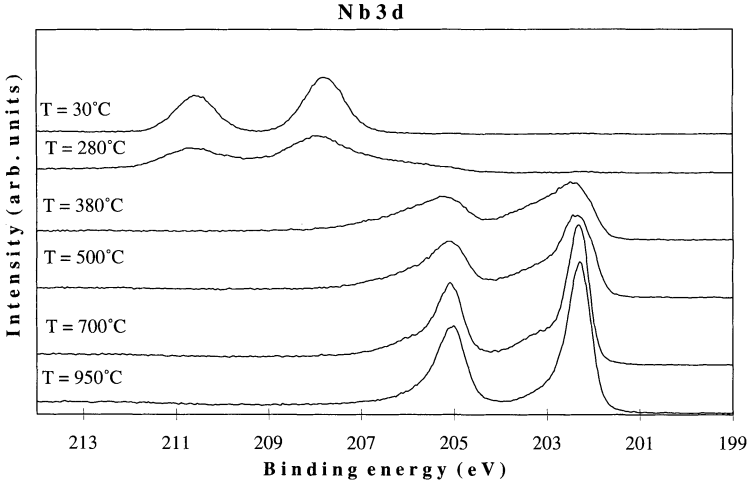

FIGURE 2 Evolution of Nb3d doublet during the heating phase, relative to the sample anodized at 5 V.

In Figure 2 the evolution with temperature of Nb3d line is represented: in the range 280–380°C there is a clear surface transition with the disappearance of the signal typical of Nb_2O_5 ($E_B = 207.5\,eV$[14]) and the appearance of the signal produced by pure niobium ($E_B = 202.3\,eV$[14]).

The C1s line is in the chemical position of amorphous carbon ($E_B = 284.5\,eV$[14]) at room temperature and it becomes niobium carbide ($E_B = 281.8\,eV$[14]) at $T = 280$–$380°C$ (Figure 3).

At the same temperatures the O1s line presents a clear reduction of the intensity and then it disappears at $T = 1000°C$ (Figure 4).

The concentrations relative to these spectra are reported in Figure 5.

The thickness vs temperature dependence obtained from the ARXPS analysis is represented in Figure 6. At room temperature the in-depth composition is the following: a layer of niobium oxide, in form of Nb_2O_5, about 60 Å thick ($\cong 15$ monolayers), upon which there is a layer of carbon, in graphitic form, whose thickness is of a few monolayers. The thickness of the Nb_2O_5 layer is consistent with that expected for an anodization of the sample at 5 V.

During the heating phase the thickness of Nb_2O_5 decreases and at $T = 280°C$ under this oxide another niobium oxide appears (NbO_2,

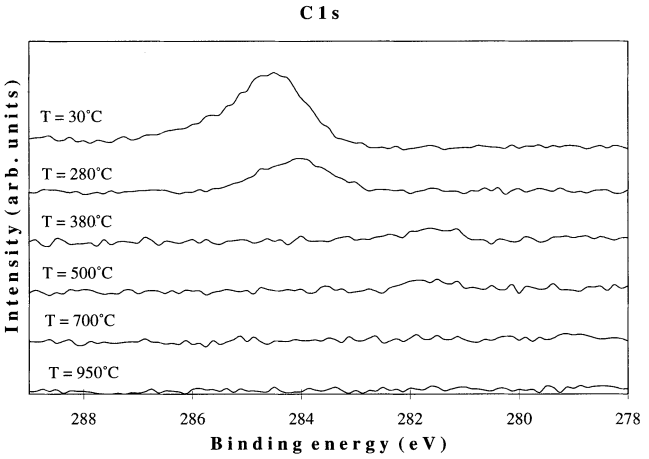

FIGURE 3 Evolution of C1s line, during the heating phase, relative to the sample anodized at 5 V.

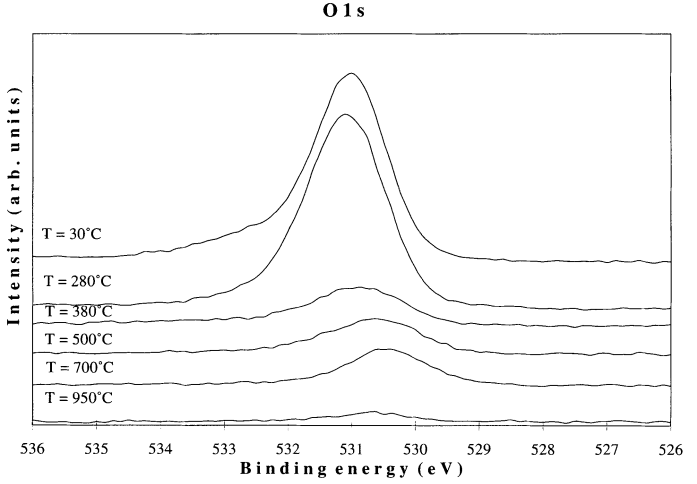

FIGURE 4 Evolution of O1s line, during the heating phase, relative to the sample anodized at 5 V.

$E_B = 206.1\,eV$[14]); NbO_2 is detectable only in the range of temperature from 280°C to 380°C. Above 380°C, under the pentoxide, the niobium monoxide (NbO, $E_B = 203.2\,eV$[14]) appears and it remains the only niobium oxide on the surface in the range 500–1000°C.

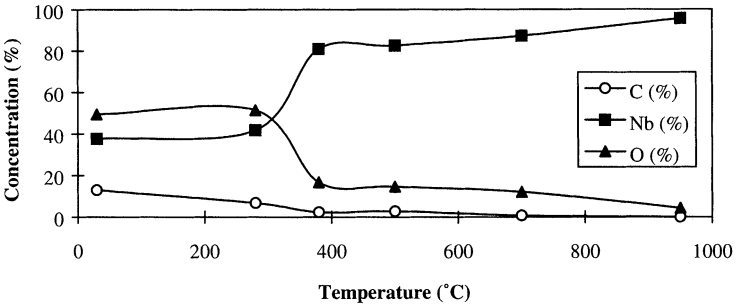

FIGURE 5 Niobium, oxygen and carbon surface concentration vs increasing temperature, for niobium anodized at 5 V (lines are a guide for the eyes).

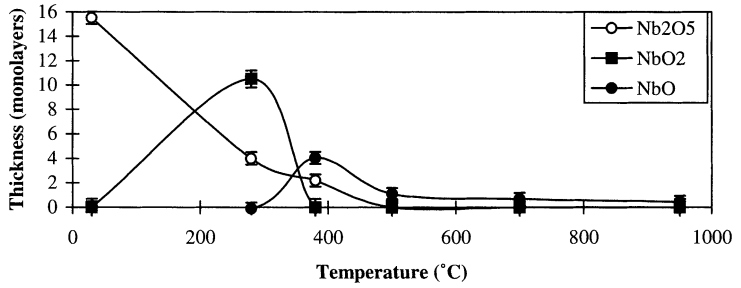

FIGURE 6 Thickness of Nb_2O_5, NbO_2 and NbO layers on niobium surface vs increasing temperature (lines are a guide for the eyes).

The angle-resolved analysis allows to establish that the layer of carbon (at room temperature of the order of 2–3 monolayers) is on the top of the niobium oxides and its thickness diminishes raising T until it disappears at 700°C (Figure 7).

B. Cooling Phase

The evolution of niobium, oxygen and carbon concentrations during the cooling down phase are reported in Figure 8.

During this phase there is an increase in the O1s line around $T = 900$°C and, in correspondence, the Nb3d line shows the doublet proper of NbO. The carbon signal is present only for $T < 500$°C as

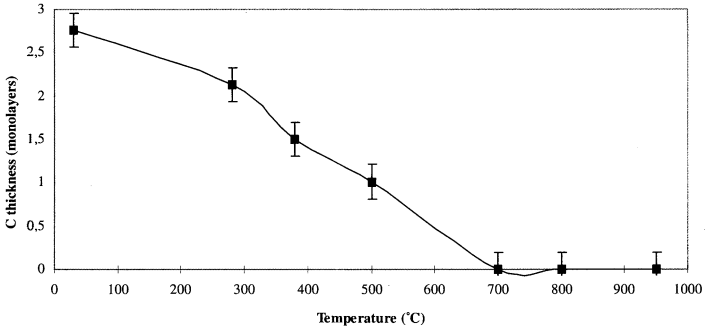

FIGURE 7 Thickness of carbon layer on niobium surface vs increasing temperature (line is a guide for the eyes).

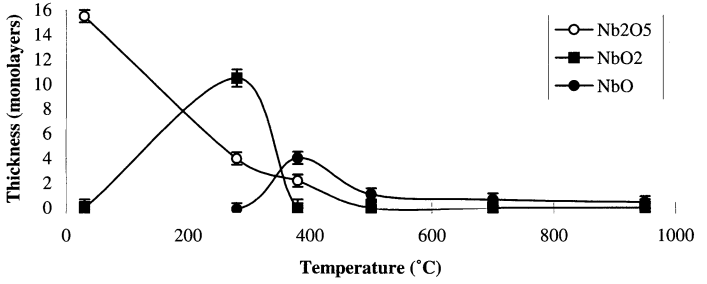

FIGURE 8 Niobium, oxygen and carbon surface concentration vs decreasing temperature, for niobium anodized at 5 V (lines are a guide for the eyes).

niobium carbide (NbC), while the graphite signal is detectable only below 200°C.

The in-depth composition deduced from angle-resolved analysis is less complex than during the heating phase: only a layer of NbO is present on niobium surface starting from 900°C; its thickness increases, diminishing T, but never reaches the initial thickness of Nb_2O_5 at room temperature (Figure 9). The carbon layer is of the order of one monolayer at room temperature (Figure 10).

C. Work Function Measurements

The work function value Φ is obtained by calculating the total width of the XPS spectrum and it is correlated with the in-depth composition

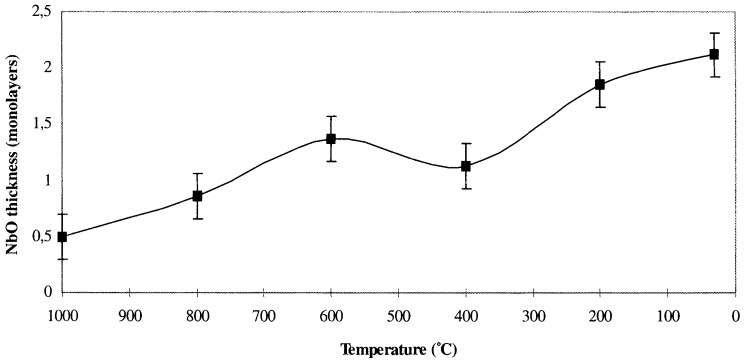

FIGURE 9 Thickness of NbO layer on niobium surface vs decreasing temperature (line is a guide for the eyes).

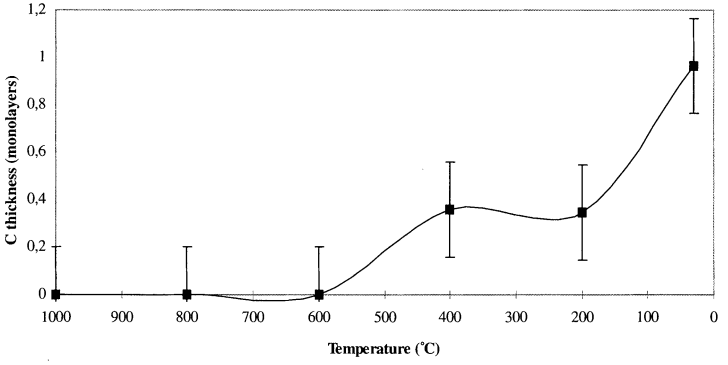

FIGURE 10 Thickness of carbon layer on niobium surface vs decreasing temperature (line is a guide for the eyes).

by alternating data acquisition with ion sputtering (Ar^+ at 2 keV). These measurements were performed on the sample anodized at 20 V and the results are represented in Figures 11 and 12: the first picture shows the work function value vs the sputtering time and the sputtering depth (the sputtering rate was about 2 Å/min, determined by the thickness of the anodic oxide layer on niobium); the second picture represents the in-depth chemical composition.

On the surface anodized and introduced in the spectrometer is present a concentration of 20 at.% of carbon and $\Phi = 3.8$ eV; after the first minutes of sputtering, the C1s signal disappears and Φ reaches its

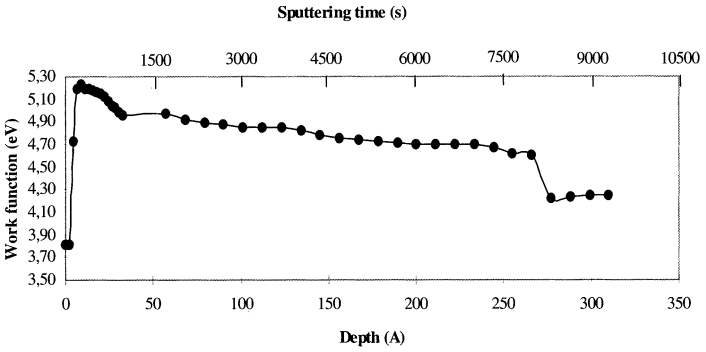

FIGURE 11 Work function vs depth, relative to a niobium sample anodized at 20 V.

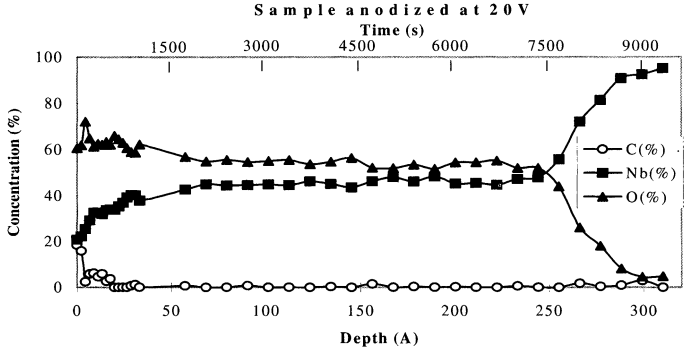

FIGURE 12 Niobium, oxygen and carbon concentration vs depth, relative to a niobium sample anodized at 20 V.

maximum value of 5.2 eV; proceeding with sputtering, Φ decreases and reaches, in correspondence of the clean surface, the value of 4.2 eV, that is near the Φ value of pure polycrystalline niobium of 4.3 eV.[17]

These measurements show that there is a correspondence between the chemical composition of the first atomic layers and the value of Φ: the main changes in Φ are all correlated with the changes in the surface concentrations of niobium, oxygen and carbon. The presence of contaminants, such as carbon, produces a remarkable decrease of Φ, while the presence of oxygen on the surface increases the work function; this is caused by the high electronegativity of oxygen,

that produces an increase of the potential barrier, generated by surface dipoles.

4. DISCUSSION

The processes concerning the first 15–20 monolayers of the niobium surface during the thermal treatments can be summarized as:

- the transition Nb_2O_5–NbO at $T \cong 280$–$380°C$;
- the disappearance of the C1s and O1s lines during the heating phase;
- the growth of the signals of oxygen and carbon, with different features, during the cooling phase.

The transition from Nb_2O_5 to NbO that involves a progressive reduction in the oxidation number of niobium (from Nb_2O_5 to NbO_2 and finally to NbO), takes place together with a change in the chemical state of carbon: this element moves from the graphitic form to a bonding state with niobium (NbC) and during this transformation there is a sharp decrease in the thickness of the carbon layer (Figure 7).

The same measurements, performed on other niobium samples obtained with different surface treatments (such as chemical polishing, exposure to air or anodization at different voltages, see Table I), show the same qualitative behavior; the main difference consists in the temperature at which the various transitions take place. In particular, concerning the transition Nb_2O_5–NbO, the temperature increases with the increasing thickness of the starting layer of Nb_2O_5: it is 200°C for a sample exposed to air, with about 10 monolayers of Nb_2O_5 at room temperature, and grows up to 380°C for a sample anodized at 20 V, on which there are about 60 monolayers of Nb_2O_5 at room temperature. The described transition is clearly irreversible as, decreasing T, after the reduction from Nb_2O_5 to NbO has occurred, we do not observe again the presence of Nb_2O_5 layer on the surface, but only of a NbO layer.

This transition is probably explained by a desorption process of CO and CO_2: oxygen atoms coming from Nb_2O_5, combine with carbon atoms, present on top of the Nb_2O_5 layer as graphite, and leave the

surface as CO or as CO_2. The transition cannot be ascribed completely to a migration to the bulk of the surface oxides: in this case for the sample anodized at 5 V under the Nb_2O_5 layer (thickness $\cong$ 15 monolayers) there should be a NbO_2 layer 25–30 monolayers thick, which is not revealed by the ARXPS analysis, as the thickness of the NbO_2 layer is only 10 monolayers (Figure 6). The assumption of a migration of oxygen towards the niobium bulk at these temperatures is improbable, owing to the low mobility of oxygen in niobium for $T < 700°C$;[18] moreover this hypothesis would not explain the contemporary decrease of the carbon signal.

During the heating phase the disappearance of the O1s signal occurs always in the range 700–1000°C for all the samples analyzed; in particular we observe that the temperature at which we register the disappearance of the signal is different for the various samples but, for every single sample, it coincides with that at which the niobium monoxide reappears during the cooling phase.

The growth of a NbO layer during the cooling phase shows different dynamic features for the different samples, that depend mainly on their initial state; the thickness of the oxide layer after one thermal cycle is, in fact, roughly proportional to the concentration of oxygen measured on the surface before the beginning of the cycle itself, while the conditions of background pressure and its chemical composition (CO, CO_2, H_2O) are independent of the sample under study.

These experimental results are in agreement with a process of oxygen migration from the bulk towards the surface during the cooling process; surely this is not the only explanation for the NbO growth, but it can largely account for the growth rate of surface oxide, too fast to be explained in terms of surface contamination from the residual gas.

The disappearance of the O1s signal during the heating phase for $T > 700°C$ can be ascribed partly to a desorption process as CO or CO_2 and partly to a diffusion process of oxygen in the niobium matrix. This is confirmed by the fact that upon 700°C there are no more traces of carbon on the surface and the oxygen cannot desorb as O_2. The desorption of oxygen in the form of NbO is also excluded for temperature below 1600–1800°C.[19]

The evolution of the carbon signal during one thermal cycle is less correlated to the sample temperature and to the sample itself: the

disappearance during the heating phase is due to the desorption of CO or CO_2, while the formation of a carbon layer below 500°C is produced by contamination from residual gas. The quantity of carbon that is present on the surface after the cooling process (2–3 at.%) is completely consistent with that revealed on a niobium sample in consequence of the contamination produced only by the residual gas.

5. CONCLUSIONS

XPS and ARXPS measurements have also been performed on other samples different from the niobium sample anodized at 5 V, to which the previous discussion refers. These samples were prepared following procedures commonly employed in standard RF cavities preparations (Table I). The results obtained underline that the surface evolution during the thermal cycles is qualitatively the same, independently from the specific surface treatment. The main difference concerns the temperatures at which we observe the surface transitions which increase with the increasing thickness of the initial layer of Nb_2O_5 on the surface.

XPS analyses performed on the various samples of niobium underline the complexity of the processes that occur during the thermal cycles. In particular this study shows that the different treatments employed in the preparations of RF cavities produce qualitatively the same chemical composition of the surface, with regard to the first twenty atomic layers, approximately and that the chemical evolution with temperature of these layers is very similar.

During the heating phase we observe an irreversible reduction of niobium from Nb_2O_5 to NbO at $T = 280–380$°C: the Nb_2O_5 layer becomes poor of oxygen, that combines with carbon and leaves the surface as CO and CO_2. The migration of oxygen as O_2 into the niobium matrix can only play a minor role as the mobility of oxygen in niobium at those temperatures is low. This process is very important for the superconducting behavior of cavities, owing to the dielectric properties of niobium pentoxide and the metallic properties of niobium monoxide, characterized by a very low critical temperature ($T_c \cong 1.4$ K).

The disappearance of the O1s line at 1000°C is caused both by a desorption process of oxygen from the surface and by the oxygen migration in the bulk. The migration in the bulk is consistent with the increase of the O1s signal during the cooling phase, that shows different dynamic features in the various samples and that cannot be caused only by the contamination produced by the residual gas.

The disappearance of the C1s line at 700°C is due to the desorption of CO and CO_2; the formation of a carbon layer, during the cooling phase, for $T < 500$°C is completely consistent with a contamination process caused by the residual gas; this growth occurs first with the formation of an NbC layer and, then, with a graphitic layer.

The work function measurements show the correlation between this quantity and the chemical composition of the surface; with a carbon layer on the niobium surface there is a decrease of 0.4 eV, with respect to the Φ value of metallic niobium. A Nb_2O_5 layer produces instead an increase of about 1 eV compared to the Φ value of 4.2 eV, typical of pure niobium.

In conclusion we observe that the thermal treatment in UHV at 1000°C allows to obtain a surface free of contaminants (oxygen and carbon), but not in a permanent way. During the cooling phase, in fact, oxygen diffuses from the bulk towards the surface and a carbon layer grows.

References

[1] H. Piel, *CAS Proc.*, CERN 89-04 (1989).
[2] W. Weingarten, CERN/AT-RT (int) 92-3 (1992).
[3] J. Halbritter, *Proc. Workshop on RF Superconductivity*, KfK 3019, 190 (1980).
[4] P. Kneisel, *Proc. Workshop on RF Superconductivity*, KfK 3019, 27 (1980).
[5] H.H. Farrell, H.S. Isaac and M. Strongin, *Surf. Sci.*, **38**, 31 (1973).
[6] M. Strongin, H.H. Farrell, H.J. Halama, O.F. Kammerer and C. Varmazis, *Partic. Accel.*, **3**, 209 (1972).
[7] P. Fabbricatore, G. Gemme, R. Musenich, R. Parodi and S. Pittaluga, *Proc. 7th Workshop on RF Superconductivity*, 385, Gif sur Yvette (1995).
[8] K. Asano, T. Furuya, Y. Kojima, S. Mitsunobu, H. Nakai, S. Noguchi, K. Saito, T. Tajima, M. Tosa and K. Yoshihara, *KEK Report* 88-2 (1988).
[9] T. Imamura and S. Hasuo, *IEEE Trans. Appl. Superconduct.*, **2**, 84 (1992).
[10] S. Doniach and M. Sunjic, *J. Phys. C Solid State Phys.*, **3**, 285 (1970).
[11] R.I. Jenrich and P.F. Sampson, *Technometrics*, **10**(1) (1968).
[12] D. Briggs and M.P. Seah, *Practical Surface Analysis by Auger and X-ray Photoelectron Spectroscopy*, Wiley, New York (1983).
[13] D.A. Shirley, *Phys. Rev. B*, **5**, 4709 (1972).
[14] J.F. Moulder, W.F. Stickle, P.E. Sobol and K.D. Bomben, *Handbook of X-Ray Photoelectron Spectroscopy*, Perkin-Elmer Corporation, USA (1992).

[15] C.S. Fadley, *Prog. Surf. Sci.*, **16**, 3 (1984).
[16] M.P. Seah and W.A. Dench, *Surf. Interface Anal.*, **1**, 2 (1979).
[17] D.E. Eastman, *Phys. Rev. B*, **1**, 1 (1970).
[18] R.A. Pasternak, *U.S. AEC Interim Report TID*-19489, 11 (1963).
[19] L.H. Rovner, D. Drowart *et al.*, *Technical Report AFML*-68-200, Air Force Material Laboratory, Wright-Patterson Air Force Base, Dayton, Ohio.